Removal of biofilms by impinging water droplets

Removal of biofilms by impinging water droplets

A. W. Cense[a] and M. E. H. van Dongen
University of Technology Eindhoven, Den Dolech 2, 5600 MB Eindhoven, The Netherlands

B. Gottenbos and A. M. Nuijs
Philips Research Laboratories, High Tech Campus 34, 5656 AE Eindhoven, The Netherlands

S. Y. Shulepov
Philips Applied Technologies, High Tech Campus 7, 5656 AG Eindhoven, The Netherlands

(Received 11 November 2005; accepted 12 August 2006; published online 22 December 2006)

The process of impinging water droplets on *Streptococcus mutans* biofilms was studied experimentally and numerically. Droplets were experimentally produced by natural breakup of a cylindrical liquid jet. Droplet diameter and velocity were varied between 20 and 200 μm and between 20 and 100 m/s, respectively. The resulting erosion process of the biofilm was determined experimentally with high-speed recording techniques and a quantitative relationship between the removal rate, droplet size, and velocity was determined. The shear stress and the pressure on the surface during droplet impact were determined by numerical simulations, and a qualitative agreement between the experiment and the simulation was obtained. Furthermore, it was shown that the stresses on the surface are strongly reduced when a water film is present. © *2006 American Institute of Physics*. [DOI: 10.1063/1.2374950]

I. INTRODUCTION

Bacterial biofilms on surfaces cause serious problems, ranging from economic damage and material damage to life-threatening diseases.

For example, biofilms on ship hulls and in pipelines increase the friction, which adversely affects the energy use. Water filters and pipelines can become clogged and can eventually fail due to biofilm formation. In health care, biofilm growth on implants, such as artificial heart valves, can be life threatening. A common biofilm related illness is caries, which is the formation of cavities (holes) in teeth due to acids that are produced by specific bacteria of which biofilms are built up.

These oral biofilms, also referred to as dental plaque, are normally removed mechanically by means of tooth brushes, tooth picks, and tooth floss. Another mechanical method that can be used to remove biofilms is by applying a water spray, where the water droplets of which the spray consists have a diameter between 5 and 200 μm and a velocity between 20 and 150 m/s.[1]

It is generally known that high-velocity water droplet impact can create damage to aircraft, missiles, and turbine blades. The research on high-speed droplet impact, where we define high speed as velocities being greater than 150 m/s, has therefore received a lot of attention.[2–5] Low speed droplet impact (i.e., velocities smaller than 20 m/s) is relevant in the field of ink-jet printing, spray painting, and agriculture (pesticide distribution). Most studies on low-speed droplet impact focus on the spreading and splashing of droplets.[6,7] Surprisingly, the field between high-speed and low-speed droplet impact (i.e., velocities between 20 μm and 150 m/s) did not receive much attention in the past.

In this article we present an experimental and numerical study on droplet impact for the removal of biofilm layers. Where previous studies focused on relatively large droplets with diameters ranging between 0.5 and 10 mm, we analyzed the impact of small droplets with diameters between 20 and 200 μm at velocities between 20 and 100 m/s.

II. MATERIALS AND METHODS

A. Droplet generator

"Monodisperse" droplets are produced by means of a cylindrical liquid jet that breaks up due to the growth of natural instabilities on the surface of the jet.[8]

Experimentally, circular jets were produced with the setup that is shown in Fig. 1. A 1 l reservoir (304L-HDf4-

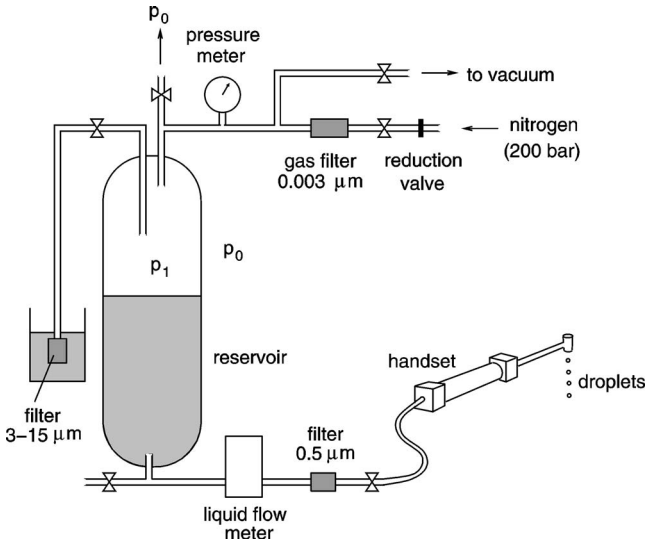

FIG. 1. Experimental setup to generate monodisperse droplets.

[a]Electronic mail: arjen.cense@gmail.com

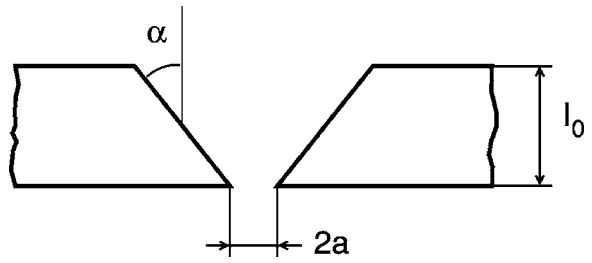

FIG. 2. Nozzle dimensions. l_0 is the length of the nozzle, a is the radius, and α is the angle of the inlet.

1000, Swagelok, USA), filled partly with pure water, is pressurized with nitrogen from a cylinder. Nitrogen is first filtered through a filter with a pore size of 0.003 μm (Wafergard II F Micro, Swagelok, USA). Pure water (Sigma-Aldrich, The Netherlands) is filtered through a glass filter with a pore size of 3–15 μm (Schott, Germany). The water goes to the nozzle through a 0.5 μm filter (F Series, Swagelok, USA) and a liquid mass flow meter (Liqui-Flow meter L2, Bronckhorst Hi-Tec, The Netherlands) that measures flow rates between 4 and 200 g/h. A 0.8 mm diameter tube, 1.2 m in length connects to a handpiece, which holds the nozzle.

The nozzles are platinum microscope apertures (Agar Scientific, United Kingdom), which are glued in nozzle holders. The nozzles have diameters of 10 μm (A0301P), 25 μm (A0303P), 50 μm (A0306P), and 100 μm (A0309P). The nozzle geometry of the apertures is shown in Fig. 2. Table I gives the characteristic properties of the nozzles and the range of Reynolds numbers in which they were used, where the Reynolds number is defined as $\mathrm{Re}=U2a/\nu$. Here, U is the jet velocity, a is the aperture radius and ν is the kinematic viscosity, which is 10^{-6} m^2 s^{-1} for water. The nozzle and the holder are assembled in a handset with an O-ring and a nozzle plug.

The droplet sizes were determined visually using a flash lamp (Fisher Nanolite No. 151, High-Speed Photo-Systeme, Germany) a microscope objective (5×, numerical aperture (NA) 0.12 and 20×, NA 0.40, Leica, Germany) and a charge coupled device (CCD) camera (CV-M10 BX, JAI, Denmark). The exposure time is determined by the discharge of the lamp, which equals 18 ns. Images were processed automatically in MATLAB (version 7, The MathWorks, USA), and the mode (the mode of a distribution is defined as the most frequently occurring droplet size) of the droplet distribution was determined for various reservoir pressures, see Table II.

TABLE I. Properties of the platinum nozzles. The nozzle radius is a, the length of the inlet is l_0, α is the angle of the inlet, and $\mathrm{Re}_{\min}$ and $\mathrm{Re}_{\max}$ are the minimum and maximum Reynolds number at which the nozzles were used.

a (μm)	l_0 (μm)	$l_0/2a$ (–)	α (°)	$\mathrm{Re}_{\min}$ (–)	$\mathrm{Re}_{\max}$ (–)
5	85	8.5	28	300	840
12.5	80	3.2	49	750	2100
25	80	1.6	53	1500	4200
50	60	0.6	53	3000	8400

TABLE II. Modes of the droplet size distribution in microns as a function of pressure, p, and nozzle radius, a. The last column represents the average full width at half maximum (FWHM) of the droplet distributions corresponding to the corresponding nozzle size.

a (μm) ↓ p (10^5 Pa) →	5	10	15	20	25	30	35	FWHM (μm)
5	23	21	21	19	19	19	17	3
12.5	50	49	49	51	52	53	51	6
25	94	94	92	113	112	111	111	25
50	181	166	166	163	164	164	168	20

B. Biofilm

Layers of biofilm are grown on a Petri dish (⌀125 × 25 mm, Corning, USA) by adding *Streptococcus mutans* bacteria (ATCC 700610, LGC Promochem, United Kingdom) to growth medium (brain heart infusion, Sigma-Aldrich, The Netherlands) supplemented with 2% sucrose (Sigma-Aldrich, The Netherlands). The bacteria attach on the polystyrene surface of the Petri dish where they grow with the aid of the nutrients that are provided from the growth medium. For two consecutive days, the growth medium is refreshed and new bacteria are added twice a day. The resulting biofilm is approximately 60–80 μm thick.

Biofilms were mechanically characterized with a microindentation technique. It was found that the biofilm is a viscoelastic solid, with a storage modulus between 1 and 8 kPa and a loss modulus between 5 and 10 kPa at a strain of 10%.[9]

C. Visualization of the erosion process

A Petri dish with biofilm was placed in a custom made holder on the stage of a microscope (DM LM, Leica, Germany). The sample was illuminated from below with a 100 W mercury lamp (HBO 100 W/2, Leica, Germany) through a condensor (Leica, 0.20–1.25 Oil S1). The biofilm was subjected to droplets from the cylindrical jet. The impact site on the biofilm was imaged through a long distance objective (5×, NA 0.25, Leica) through the microscope on the CCD of a high speed camera (Ultima APX, Photron, United Kingdom). The microscope was positioned horizontally to prevent that a water film would build up on the biofilm which could possibly interfere with the measurement. For this purpose, an aluminum frame was built to hold the microscope. The setup is shown in Fig. 3.

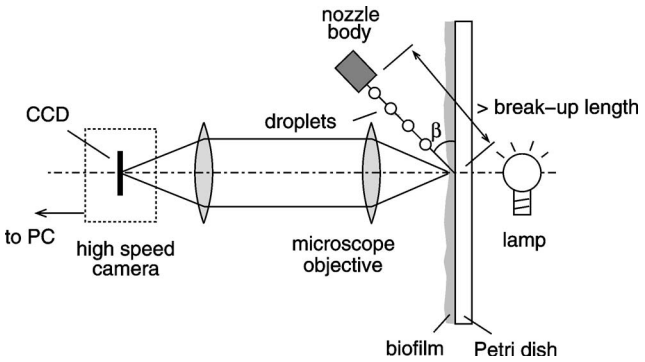

FIG. 3. Schematic of the experimental setup.

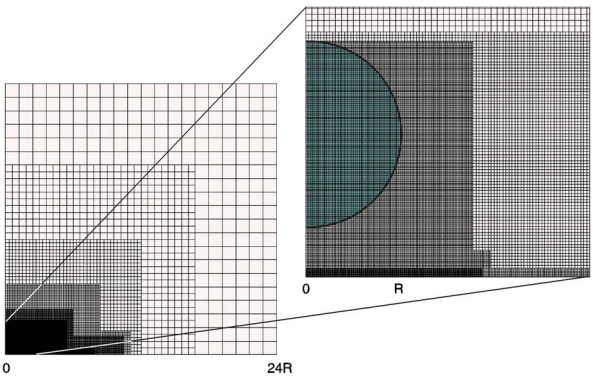

FIG. 4. (Color online) Mesh of the numerical domain. The mesh is refined at the position of the droplet and near the wall. Cells are hexahedral everywhere, but prismatic at the symmetry axis.

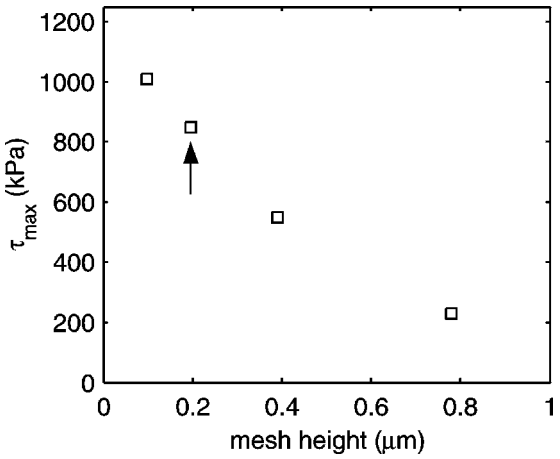

FIG. 5. The maximum value of the shear stress at the wall during droplet impact is shown as a function of the mesh height. The arrow indicates the mesh size at which the remaining simulations have been performed. Droplet radius is 100 μm, droplet velocity is 50 m/s.

The pressure in the reservoir was set to the desired value and the droplets were aimed at the biofilm at an angle β with the biofilm. It was possible to adjust the angle of impact from 10° to 60° (perpendicular impact is by definition 90°). The high-speed camera was operated at a shutter time of 4 μs and at a frame rate of 10 000 frames per second.

The valve to the nozzle was opened and the droplets from the jet were initially blocked manually with a metal plate. Once an undamaged piece of the biofilm was positioned under the microscope objective, the metal plate was removed and a stream of droplets was allowed to make impact with the biofilm. The first 150 frames (≡15 ms) of the impact process were stored in avi format (uncompressed) on a standard personal computer.

Images were processed with Image Pro Plus (version 4.5, Media Cybernetics, USA). The size of the cleaned area was measured. A gray-value threshold was used to distinguish between biofilm and cleaned polystyrene. The threshold was chosen manually. As the illumination was kept constant between a series of measurements, it allowed a proper comparison between the different settings. Images in which droplets were in between the objective and the cleaned area were not taken into account for the measurement.

At each setting of the velocity and the diameter, four to six sites on the biofilm were treated. The results were then averaged and the standard deviation was calculated.

D. Numerical simulations

Simulations of droplets impinging on a solid surface were performed with STAR-CD (version 3.15, Adapco Group, London, England).[10,11] Three-dimensional incompressible simulations were done on a cylindrical symmetric mesh. A wedge shaped computational domain was used with an angle of 3°, consisting of hexahedral cells (six sides) and a layer of prismatic cells (five sides) at the central axis of symmetry. An angle of 5° did not yield different results.

The computational domain measured 24×24 droplet radii (see Fig. 4). A fixed grid was used with mesh refinement in the regions that needed more detail, such as near the air-liquid interface and the wall boundary. At the location of the droplet, the mesh consisted of 62 cells per radius (cpr). Near the wall the mesh was refined to 124 cpr.

It was found that the results depended on the mesh size. By performing simulations at decreasing mesh sizes it was concluded that the maximum shear stress linearly converges if the mesh size goes to zero (see Fig. 5). At a mesh size of 124 cpr the shear stress at the wall is underestimated by approximately 30%. This factor was taking into account for the calculation of the true shear stress. No grid dependence was found for the pressure. All simulations were performed using the same grid refinement (indicated by the arrow).

For this specific simulation it was verified that no significant different results were obtained when the time step was decreased from 2×10^{-8} s to 10^{-8} s. In general, all simulations were carried out with the same dimensionless time step, which was $\Delta t \approx 4 \times 10^{-3} r_0 / U_0$. Here r_0 represents the droplet radius and U_0 the impact velocity. All the computations have been carried out on AMD Opteron 252 64 bits dual processor nodes of a Linux based cluster.

A so-called volume of fluid (VOF) method[12] was used to conduct simulations involving free surface flows with sharp interfaces. Per grid cell, in addition to quantities such as pressure and velocity, a scalar quantity is introduced, which represents the fraction of the two fluids. If a cell is filled entirely with liquid, the VOF fraction is 1; if a cell is filled completely with gas, the VOF fraction is 0. For cells that are partly filled with liquid, the VOF scalar takes a value between 0 and 1, in accordance with the liquid fraction. The VOF fraction is transported by means of the advection equation. Furthermore, surface tension and viscosity were taken into account in the simulations.

In the first series of simulations, the pressure and the shear stress at the wall were recorded as a function of time for various droplet velocities and droplet diameters. Droplet velocities ranged from 30 and 100 m/s and droplet radii ranged from 10 to 100 μm.

In a second series of simulations, a thin layer of water with thickness h was put on the substrate. The effect of the water layer thickness on the pressures and shear stresses on the solid surface was determined. Table III shows an overview of the numerical experiments.

TABLE III. Overview of numerical simulations of droplet impact on water layers with height h .

Droplet radius r_0 (μm)	Impact velocity U_0 (m/s)	h/r_0
100	50	0
100	50	0.015
100	50	0.03
100	50	0.05
100	50	0.1
100	50	0.2

III. EXPERIMENTAL RESULTS

The removal process of the biofilm by impinging droplets from a monodisperse droplet stream can be characterized by two phases, namely penetration and growth as schematically indicated in Fig. 6. Penetration is the process in which the biofilm is removed until the polystyrene surface is reached; growth is the process in which the existing hole in the biofilm grows.

A. A threshold velocity for cleaning

A critical velocity is needed to remove the biofilm. It was visually observed that the top layer of the biofilm is removed at velocities as low as 15 m/s. The bottom layer is much more rigid and threshold velocities for removal are typically 30 m/s. We define the cleaning threshold velocity

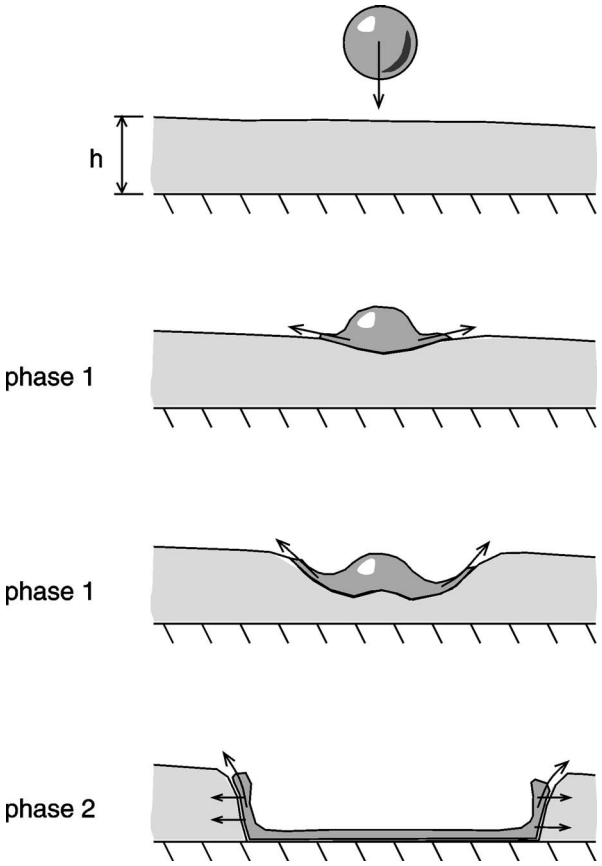

FIG. 6. Schematic representation of the removal process of the biofilm with droplets. Phase 1 is penetration of the biofilm. Phase 2 is growth of the cleaned area. Biofilm has thickness h.

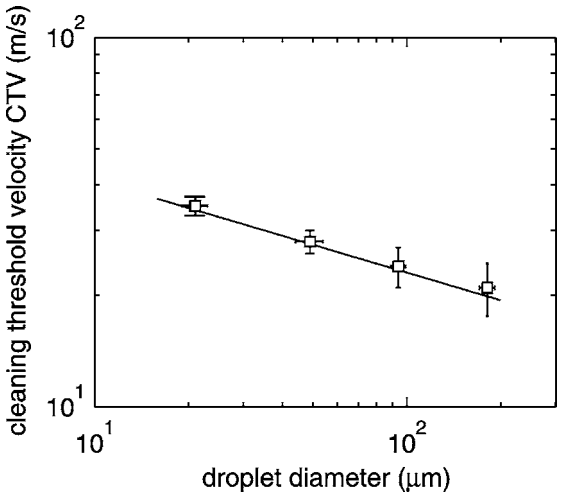

FIG. 7. CTV as a function of the droplet diameter d_0.

(CTV) as the velocity at which no removal of the biofilm to the polystyrene is achieved after a prolonged exposure to the droplets, which was typically 10 s or more. The CTV is shown as a function of droplet diameter d_0 in Fig. 7. The CTV follows a $d_0^{-1/4}$ proportionality.

The cleaning threshold velocity is defined in analogy with the damage threshold velocity (DTV), first introduced by Seward *et al.*,[13] and later used by Coad *et al.*[14] and Kennedy and Field[15] for studies of brittle materials. The damage threshold velocity was defined as the velocity threshold at which damage is first observed. They found a stronger relationship between the droplet diameter and the damage threshold velocity; their DTV showed a $d_0^{-1/3}$ proportionality.

B. Penetration phase

At each setting of d_0 and U_0, different sites on the biofilm were treated. We measured the time until a hole was visible and multiplied this with the droplet frequency, which depends on the flow rate Q and on the droplet diameter d_0 as

$$f = \frac{Q}{\frac{1}{6}\pi d_0^3} = \frac{6a^2 U_0}{d_0^3} \sim \frac{U_0}{d_0}, \tag{1}$$

where a is the radius of the nozzle. Typical frequencies for our setup are 50–1000 kHz. The critical number of droplets, N_{crit}, needed to penetrate the biofilm layer was thus obtained. The average and the standard deviation were calculated, and the results are shown in Fig. 8. Figure 8(a) shows N_{crit} as a function of the velocity for four droplet sizes; Fig. 8(b) shows N_{crit} as a function of the droplet size for one velocity.

The general trend is that N_{crit} decreases for larger impact velocities for all droplet diameters [Fig. 8(a)]. A similar trend, but now as a function of the droplet size, is observed in Fig. 8(b).

The amount of liquid that is needed to clean a certain area, just by penetrating through the biofilm layer, depends on the droplet size. Assume that the size of the initial hole is proportional to the droplet's cross-sectional area $\sim d_0^2$. The volume needed to penetrate through the biofilm layer is proportional to $N_{crit} d_0^3$. To clean a specific area A, we need a

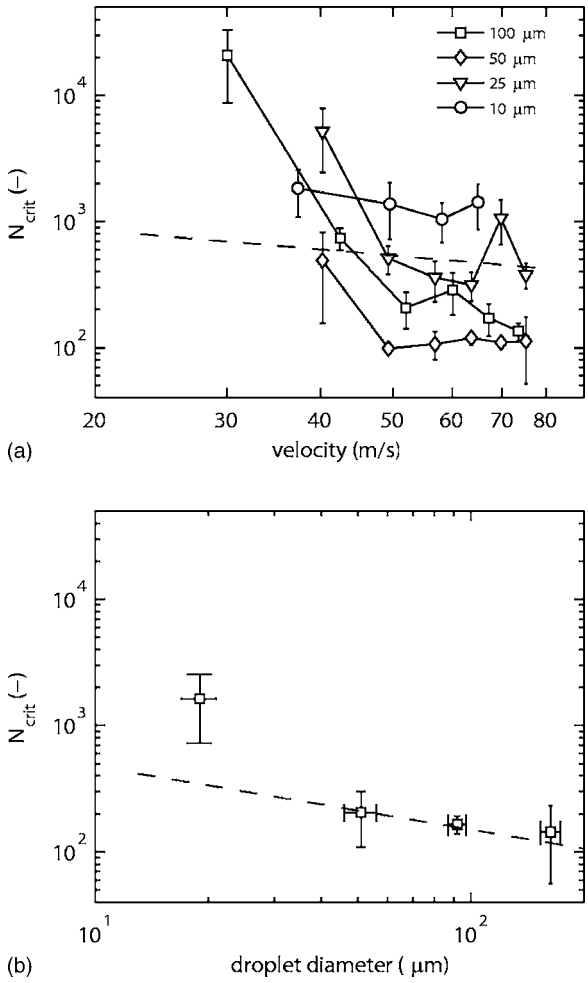

FIG. 8. Critical number of impacts N_{crit} necessary to penetrate the biofilm to the polystyrene. (a) Each curve represents results for one nozzle diameter, indicated by the legend (in microns), as a function of droplet velocity. (b) N_{crit} as a function of droplet size, for constant velocity (61 m/s). Angle of impact is 60°. Note that a double logarithmic scale is used. Dashed lines indicate expected dependence according to numerical simulation.

number of spots proportional to A/d_0^2. This requires a total liquid volume of the order of $AN_{crit}d_0$. In Fig. 9, the parameter $N_{crit}d_0$ is plotted as a function of the droplet size. The error bars are rather large, but an optimum appears to lie at $d_0=50$ μm. Summarizing: to clean a given area A by penetration only, droplets with a diameter of 50 μm require the smallest volume.

C. Growth phase

The nozzle diameter and the angle of impact remained constant, while the velocity of the droplets was changed. Figure 10 shows the cleaned area as a function of the number of droplet impacts for different velocities, ranging from 42 to 79 m/s. The angle of impact is 60°. The nozzle radius is 25 μm.

The cleaning rate is higher for higher impact velocities. For the highest impact velocity, the diameter of the cleaned area after 15 ms (≈3000 impacts) is approximately six times the droplet diameter.

In Fig. 11 we have plotted the cleaned area scaled with the cubed impact velocity. Most curves coincide, except the

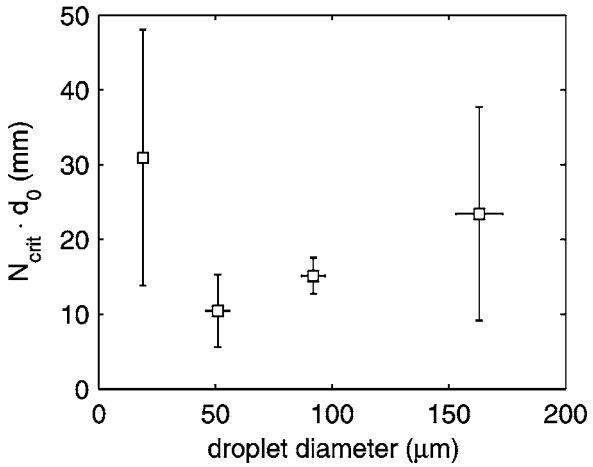

FIG. 9. The volume needed to clean a certain area only by penetration is proportional to $N_{crit}d_0$. Impact velocity was for all droplets 61 m/s.

curve belonging to an impact velocity of 42 m/s. Results for the 10, 25, and 100 μm diameter nozzles also show a good correspondence between the cleaned area and the impact velocity cubed (not shown).

In a different set of experiments the droplet size was varied at a constant velocity. Figure 12 shows the cleaned area A_1 normalized with the droplet's cross-sectional area as a function of the number of droplet impacts for droplets of different sized nozzles at an impact velocity of 61 m/s. The growth rate scales roughly with d_0^2.

As the droplet volume scales with d_0^3, the cleaned area per liquid volume scales approximately with $1/d_0$. Thus, once a hole is formed in the biofilm, smaller droplets clean at a higher rate than larger droplets with respect to the used volume.

IV. NUMERICAL SIMULATIONS

It can be expected that the impact pressure scales with the Bernoulli pressure ρU_0^2, with ρ the density of water. This

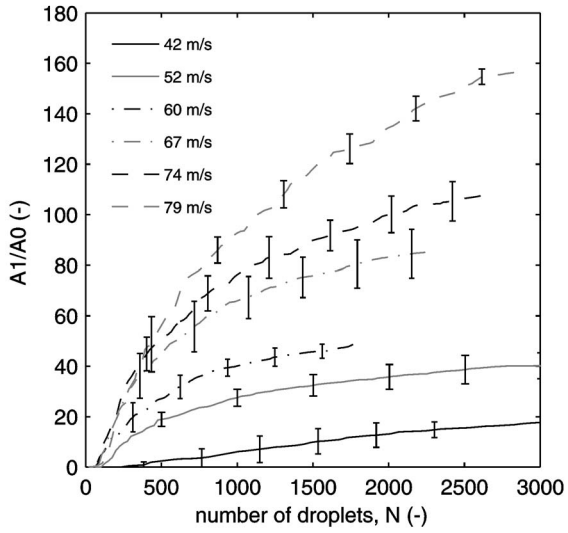

FIG. 10. Cleaned area A_1 normalized with the nozzle area A_0 as a function of the number of droplet impacts N for different impact velocities, indicated by the legend. Nozzle diameter equals 50 μm. Mode of the droplet size depends on the velocity and is approximately 100 μm; angle of impact is 60°. Error bars indicate one standard deviation over 4–6 experiments.

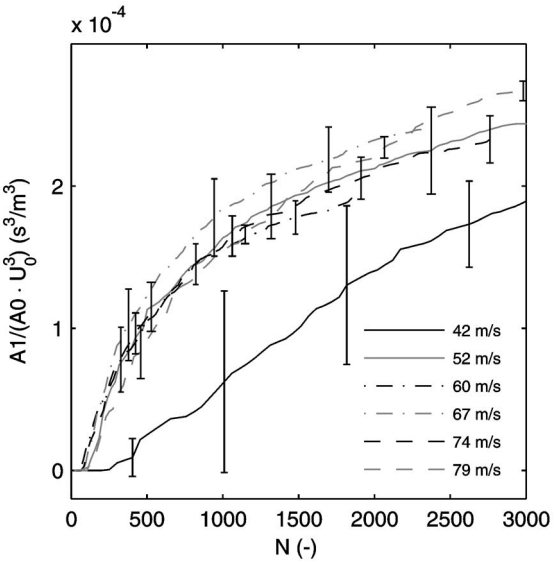

FIG. 11. Normalized cleaned area scaled with U_0^3 as a function of the number of droplet impacts N for different impact velocities, indicated by the legend. Mode of the droplet size depends on the velocity, but is approximately 100 μm; angle of impact is 60°.

is indeed confirmed by the simulation, as is shown in Fig. 13, where the impact pressures for different droplet radii is scaled with ρU_0^2. The pressure profiles are shown for different nondimensional times, which are made dimensionless by multiplying the time with the ratio of droplet velocity and droplet radius, U_0/r_0. The pressure goes to infinity at the moment of impact, but soon drops to realistic values. This anomalous behavior is due to the fact that compressibility effects are not taken into account. The pressure maximum travels radially outwards in time. This behavior is observed in various other studies.[16]

The shear stress can be expected to scale with the ratio of the impact velocity U_0 and the instationary boundary layer

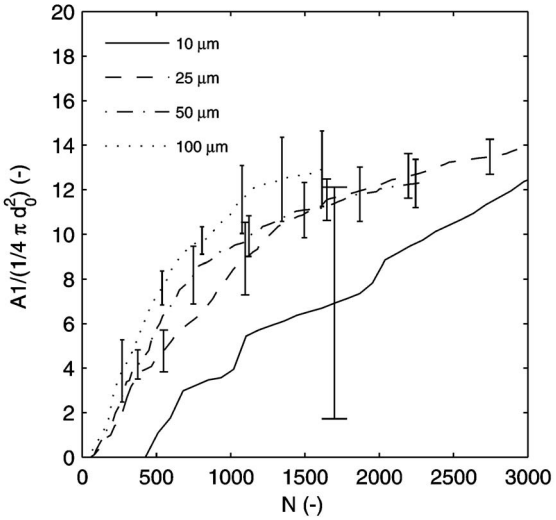

FIG. 12. Cleaned area A_1 as a function of the number of droplet impacts N for different nozzle diameters, as indicated by the legend, normalized with the droplet's cross-sectional area, $(1/4)\pi d_0^2$. Corresponding droplet sizes are 19, 51, 92, and 163 μm; droplet velocity is constant, U_0=61 m/s; angle of impact is 60°.

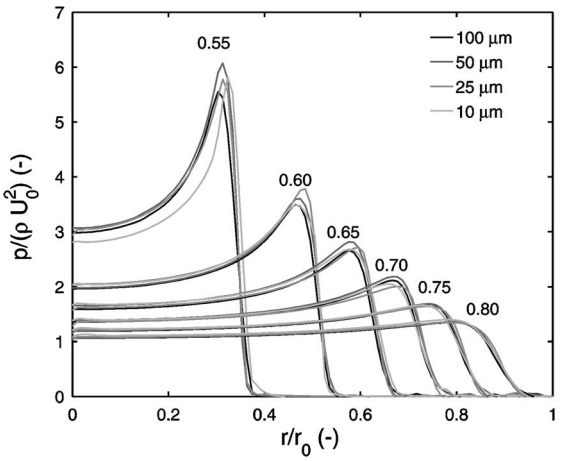

FIG. 13. Dimensionless pressure distribution at the wall at various dimensionless times for a droplet with a velocity of 50 m/s. The four curves represent different droplet radii r_0 (in microns), as indicated by the legend.

thickness. The latter grows in time according to $4\sqrt{\nu t}$, where ν is the kinematic viscosity. For t we use the characteristic impact time of the droplet, which is given by the ratio of droplet radius and droplet velocity: r_0/U_0. The shear stress thus scales as

$$\tau = \mu \frac{dU}{dy} \sim \mu \frac{U_0}{4\sqrt{\nu t}} \sim \left(\frac{\mu \rho U_0^3}{r_0} \right)^{1/2}, \tag{2}$$

where y is the axial coordinate and the equality $\nu = \mu/\rho$ was used, with μ the dynamic viscosity. This scaling is expected to be correct if $4\sqrt{\nu t} \ll r_0$, i.e., if

$$\frac{1}{4}\left(\frac{U_0 r_0}{\nu} \right)^{1/2} \gg 1. \tag{3}$$

A typical result for the shear stress on the wall as a function of time for different droplet radii is shown in Fig. 14. Results for different droplet velocities are found to be similar (not shown). The shear stress profiles do not fully satisfy similarity, which can be explained by the limited va-

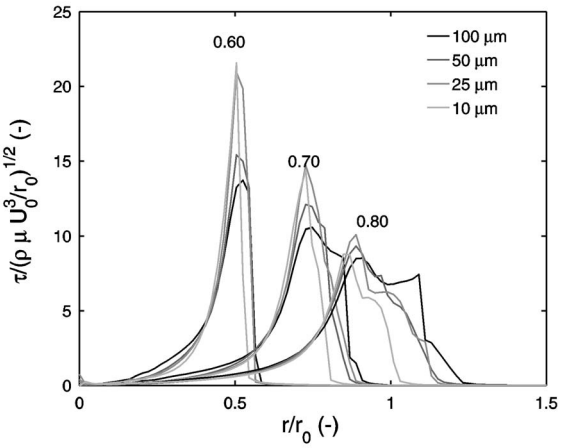

FIG. 14. Dimensionless shear stress distribution at the wall at various dimensionless times for a droplet with a velocity of 50 m/s. The four curves represent different droplet radii r_0 (in microns), as indicated by the legend.

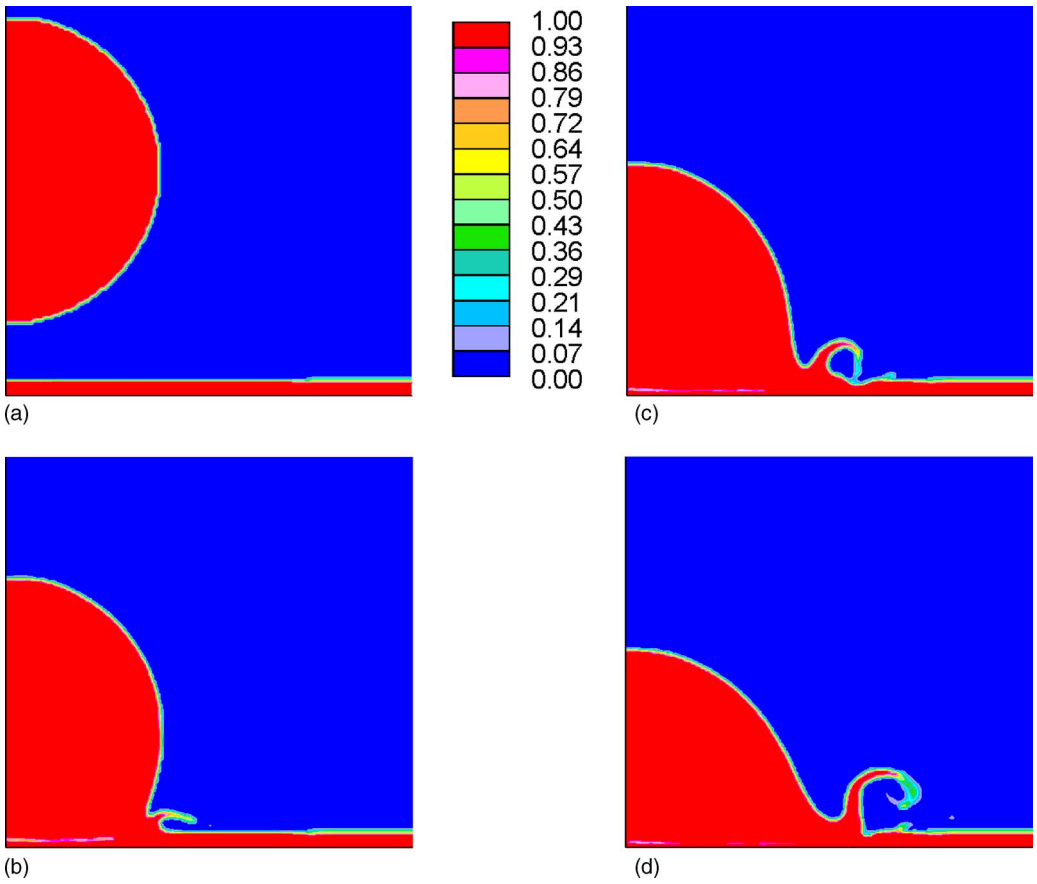

FIG. 15. (Color online) VOF fractions of an impacting water droplet with radius 100 μm and velocity 50 m/s on a 10 μm thick water film at times (a) t =0.1, (b) 1.5, (c) 2.0, and (d) 2.5 μs.

lidity of condition (3). The shear stress is zero at the center of impact and the maximum travels radially outwards with the moving contact line.

Simulations were performed with droplets impinging on thin water films. This is relevant as in reality droplets nearly always make impact on a thin water layer which is left behind from previous droplet impacts. It is of interest to know

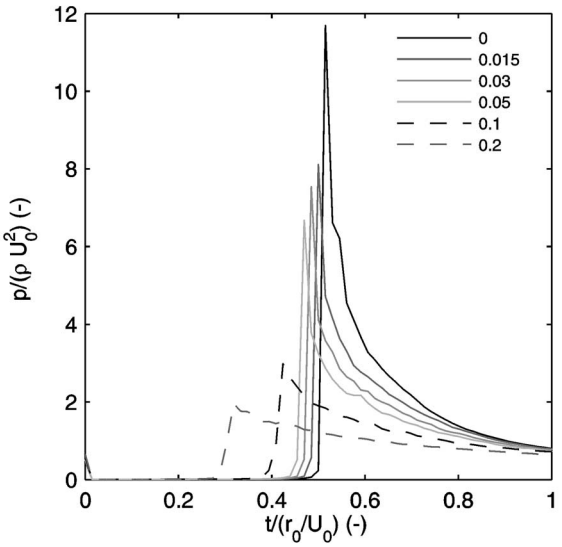

FIG. 16. The maximum dimensionless pressure along the solid surface during droplet impact as a function of the dimensionless time for different film thicknesses. The legend indicates the ratio between water layer thickness and droplet radius. A ratio of zero corresponds to impact on a dry surface. Droplet radius is 100 μm and droplet velocity is 50 m/s.

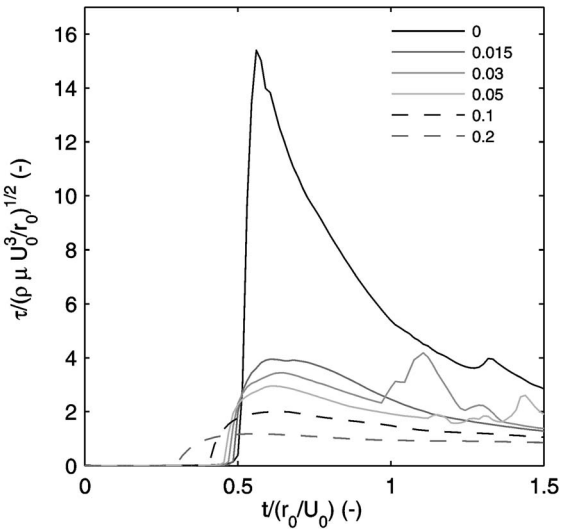

FIG. 17. The maximum dimensionless shear stress along the solid surface during droplet impact as a function of the dimensionless time for different water film thicknesses. The legend indicates the ratio between water layer thickness and droplet radius. Droplet radius is 100 μm and droplet velocity is 50 m/s.

the effect of such a thin film on the stresses on the solid surface. An example of a droplet with a radius of 100 μm impacting on a 10 μm thick water layer with a velocity of 50 m/s is shown in Fig. 15. The VOF fraction is shown, which equals one for water and zero for air. The droplet splashes in the water layer, resulting in a sheet of water that erupts from the contact line between the water and the droplet. The sheet impinges again on the water layer at a later stage. The angle at which the jet erupts becomes larger as the water layer thickness increases. In some cases, filaments break off at the top of the rim of the jet, which in reality leads to the formation of drops. This is referred to as crown formation (see, e.g., Ref. 17).

Figure 16 shows the maximum pressure along the solid surface in time for various film thicknesses, ranging from $h/r_0=0$ (dry surface) to $h/r_0=0.2$. The pressure decreases with increasing film thickness. The maximum pressure is observed in all cases just after the initial contact of the droplet with the water layer.

Whereas the effect of the water film on the pressure is relatively moderate, the effect of it on the shear stress is much more pronounced, as can be seen from Fig. 17. The maximum shear stress along the solid boundary is shown in time. A water film thickness as small as 1.5 μm ($h/r_0=0.015$) reduces the maximum shear stress of a 100 μm radius droplet impinging with a velocity of 50 m/s already by a factor of 3. The presence of a water film thus has an important influence on the shear stresses on the surface.

V. DISCUSSION AND CONCLUSIONS

The removal of biofilms with monodisperse droplet streams was studied in the laboratory. An experimental setup was built and a methodology was developed to characterize the efficacy of biofilm removal by droplets.

The numerical simulations showed that the pressure profiles at the wall in time for an impinging droplet scales with the Bernoulli pressure ρU_0^2. The shear stress at the wall in time scales to a good agree with $(\mu\rho U_0^3 r_0^{-1})^{1/2}$.

The number of droplets needed to penetrate a biofilm layer decreases with increasing droplet size and with increasing droplet velocity. If the shear stress τ is responsible for penetration, the critical number of droplets needed would follow a $U_0^{-3/2} r_0^{1/2}$ proportionality, but this is not observed (see Fig. 8). A better quantity is the shear stress integrated in time, or the impulse, $\hat{p}$:

$$\hat{p}(r) = \int_{t=0}^{\infty} \tau(r,t)dt, \tag{4}$$

which is proportional to $U_0^{1/2} r_0^{1/2}$. In this case, the critical number of droplets follows a $U_0^{-1/2} r_0^{-1/2}$ proportionality, which qualitatively is in agreement with the observations in Figs. 8(a) and 8(b) (dashed lines).

It was found that the cleaned area in the growth phase scales with the velocity of the droplets cubed and approximately with the diameter of the droplets squared. The latter observation indicates that the removal efficacy is higher for smaller droplets with respect to their volume once a hole in the biofilm is established.

Numerical simulations show that a thin water layer on the substrate reduces the pressures moderately and the shear stresses considerably.

ACKNOWLEDGMENT

This work was financially supported by Philips Oral Healthcare.

[1] A. Cense, Ph.D. thesis, Technische Universiteit Eindhoven, 2005.
[2] M. Lesser, Proc. R. Soc. London, Ser. A **377**, 289 (1981).
[3] J. Dear and J. Field, J. Appl. Phys. **63**, 1015 (1988).
[4] J. Field, Wear **233**, 1 (1999).
[5] N. Bourne, Proc. R. Soc. London, Ser. A **461**, 1129 (2005).
[6] M. Pasandideh-Fard, Y. Qiao, S. Chandra, and J. Mostaghimi, Phys. Fluids **8**, 650 (1996).
[7] D. van Dam and C. Le Clerc, Phys. Fluids **16**, 3403 (2004).
[8] S. Middleman, *Modelling Axisymmetric Flows, Dynamics of Films, Jets, and Drops* (Academic, San Diego, 1995).
[9] A. Cense, B. Gottenbos, E. Peeters, F. Baaijens, and M. van Dongen, J. Microbiol. Methods **67**, 463 (2006).
[10] CD-Adapco Group, *Methodology STAR-CD v. 3.20* (2004).
[11] J. Ferziger and M. Peric, *Computational Methods for Fluid Dynamics* (Springer, Berlin, 2002).
[12] C. Hirt and B. Nichols, J. Comput. Phys. **39**, 201 (1981).
[13] C. Seward, E. Coad, C. Pickles, and J. Field, Proc. SPIE **2286**, 285 (1994).
[14] E. Coad, C. Pickles, C. Seward, G. Jilbert, and J. Field, Proc. R. Soc. London, Ser. A **454**, 213 (1997).
[15] C. Kennedy and J. Field, J. Mater. Sci. **35**, 5331 (2000).
[16] W. Adler, in *Treatise on Materials Science and Technology*, edited by M. Preece (Academic, New York, 1979), Vol. 16, pp. 127–183.
[17] S. Lin and R. Reitz, Annu. Rev. Fluid Mech. **30**, 85 (1998).